EMBRY-RIDDLE
Aeronautical University™
SCHOLARLY COMMONS

Physical Sciences - Daytona Beach

College of Arts & Sciences

3-15-2005

Observational Investigations of Gravity Wave Momentum Flux with Spectroscopic Imaging

J. Tang
University of Illinois at Urbana-Champaign

G. R. Swenson
University of Illinois at Urbana-Champaign

Alan Z. Liu
Embry Riddle Aeronautical University - Daytona Beach, liuz2@erau.edu

F. Kamalabadi
University of Illinois at Urbana-Champaign

Follow this and additional works at: https://commons.erau.edu/db-physical-sciences

Part of the Physical Sciences and Mathematics Commons

Scholarly Commons Citation

Observational investigations of gravity wave momentum flux with spectroscopic imaging

J. Tang, G. R. Swenson, A. Z. Liu, and F. Kamalabadi

Department of Electrical and Computer Engineering, University of Illinois at Urbana-Champaign, Urbana, Illinois, USA

[1]   We apply a newly developed gravity wave momentum flux estimation method to the mesospheric measurements obtained with colocated airglow imager and meteor radar at Maui, Hawaii (20.7°N, 156.3°W), during the Maui Mesosphere and Lower Thermosphere (Maui MALT) campaign. The method identifies individual quasi-monochromatic gravity waves with periods between 6 and ∼40 min, estimates the intrinsic wave parameters, and calculates the momentum fluxes carried by vertically propagating waves. Data taken on 28 October 2003 are analyzed in detail to reveal the relationship between momentum flux and wave parameters. The January, April, July, and October 2003 data are divided into summer and winter categories, and nightly average momentum fluxes are calculated for comparison of the seasonal wave propagation directions. Average wave momentum flux is directed to the northeast during most of the summer nights, while a southwest preference exists for the winter nights. The results extracted from Maui, Hawaii, combined with the earlier results from Starfire Optical Range, New Mexico (35°N, 107°W), and other observations, support the notion that the seasonal trend in meridional flux is a global phenomenon.

1.   Introduction

[2]   Observational studies of atmospheric gravity wave (AGW) characteristics and momentum fluxes contribute to the understanding of the dynamics in the mesosphere and lower thermosphere (MALT) region. As gravity waves propagate through a region of the atmosphere, the perturbation of local density and temperature affect the photochemistry of the reactions producing the airglow [*Schubert and Waterscheid*, 1988; *Tarasick and Hines*, 1990; *Swenson and Gardner*, 1998; *Liu and Swenson*, 2003]. Waves can be detected and their parameters estimated from the airglow intensity measurements. Various techniques have been developed for wave identification and wave parameter estimation from airglow images. *Gardner et al.* [1999] described a technique to extract cross-correlation coefficients between the vertical and horizontal wind perturbations, which are associated with the azimuthal distribution of wave energy propagation, from airglow images. This technique requires high-resolution horizontal and vertical wind measurements in order to derive wind variances for estimating nightly averaged momentum fluxes. *Swenson et al.* [1999] developed a method to identify quasi-monochromatic waves from time-differenced (TD) image sequences manually and used individual wave parameters to estimate momentum flux carried by each wave. This method depends on the background horizontal wind data for intrinsic phase speed calculation. The manual wave identification method is neither practical to apply to large amounts of data, nor is it completely objective in providing detailed information. We have developed a robust and objective technique to meet the demand in studies of gravity waves and their seasonal and geographical trends which is summarized in section 2 [*Tang et al.*, 2005].

[3]   Studies on the seasonal variation of gravity wave propagation directions have been performed by researchers from several locations [e.g., *Walterscheid et al.*, 1999; *Nakamura et al.*, 2001; *Tang et al.*, 2002]. *Tang et al.* [2002] applied the *Gardner et al.* [1999] method to 32 nights of OH imager data from 1998 to 2000 (most nights having simultaneous lidar high temporal resolution wind measurements) taken at Starfire Optical Range (SOR), New Mexico (35°N, 107°W), and studied the seasonal variations in momentum flux of high-frequency gravity waves. A directional trend found by these investigations is that the meridional component has a dominant propagation directed toward the summer pole. Most attention for the dynamic influence of gravity wave in the mesosphere has been on its zonal component. The zonal gravity wave stress directly decelerates the zonal wind and also affects the meridional circulation through the Coriolis force. The meridional gravity wave stress, often found to be comparable in magnitude to the zonal component, may affect the mean meridional circulation through wave dissipation.

[4]   During the Maui MALT campaign, OH airglow images and meteor radar winds [*Franke et al.*, 2005] were acquired from the same location. Using the newly devel-
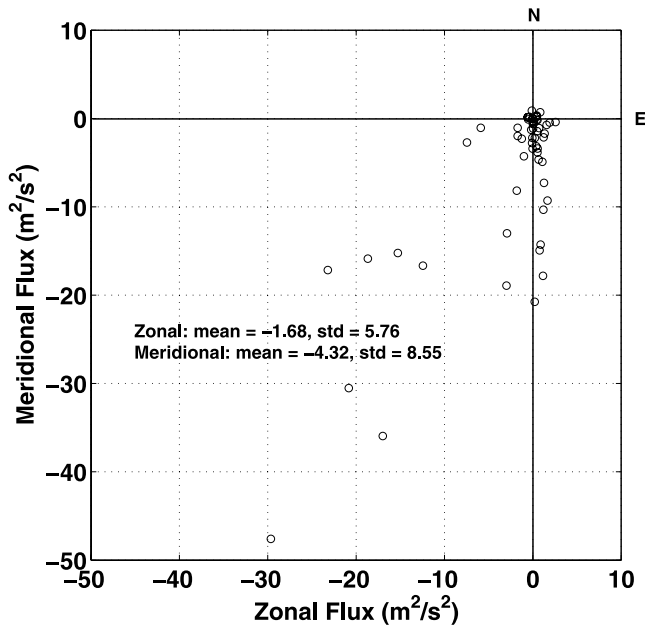
Figure 1. Scatterplot of momentum fluxes for 28 October 2003, Maui, HI. Every point represents the momentum flux carried by all propagating wave components within a 6-min time interval.

oped momentum flux extraction method, we have processed data from 2003 and analyzed the gravity wave properties and seasonal variations at Maui, Hawaii (20.7°N, 156.3°W). These results are summarized and compared with earlier results from other locations.

2. Data Processing

[5] In order to estimate momentum fluxes of gravity waves independent of high-resolution lidar (or radar) wind measurements, a new technique has been developed for extracting momentum flux from airglow images and background winds [*Tang et al.*, 2005]. This method is based on the analytical model developed by *Swenson and Gardner* [1998], which relates the perturbation in the OH volume emission rate measured from airglow images to the relative atmospheric density perturbation and consequently to the gravity wave amplitude. It estimates gravity wave momentum flux using the *Swenson and Liu* [1998] model that connects momentum flux carried by a monochromatic wave to the wave parameters including the horizontal and vertical wavelengths, the intrinsic phase speed, and the associated intensity perturbation.

[6] As described in the work of *Tang et al.* [2005], OH imager data and meteor radar data acquired simultaneously were processed to identify individual high-frequency, quasi-monochromatic gravity waves and to estimate the corresponding momentum fluxes. Keograms of the low-moon nights were made from imager data to distinguish clear nights to which the following procedures were applied. First, the raw images were preprocessed through flat-fielding, star suppression, and detrending. These steps corrected the coordinate distortion from the fish-eye lens, removed stars, and eliminated large horizontal-scale waves, respectively. Second, corrections for Doppler wind effects

were performed by pixel shifting in a group of three consecutive images using the time centered image as the base. The pixels in the first (third) image were shifted toward (against) the wind direction by linear distance translation for the time interval between the two consecutive images. The background wind for each image was generated by interpolating hourly OH layer meteor radar winds, which were weighted average of the wind altitude profiles (see *Liu and Swenson* [2003] for weighting functions). Thirdly, two TD images were created from the Doppler corrected images and common wave components were identified from the cross-periodogram of the two TD images. From the squared magnitude of the cross-periodogram, quasi-monochromatic wave components were identified and horizontal wavelengths, wave front azimuth angels, and wave amplitudes were extracted. The intrinsic phase speeds and wave propagation directions were extracted from the phase of the cross-periodogram. With the wave amplitudes in TD images
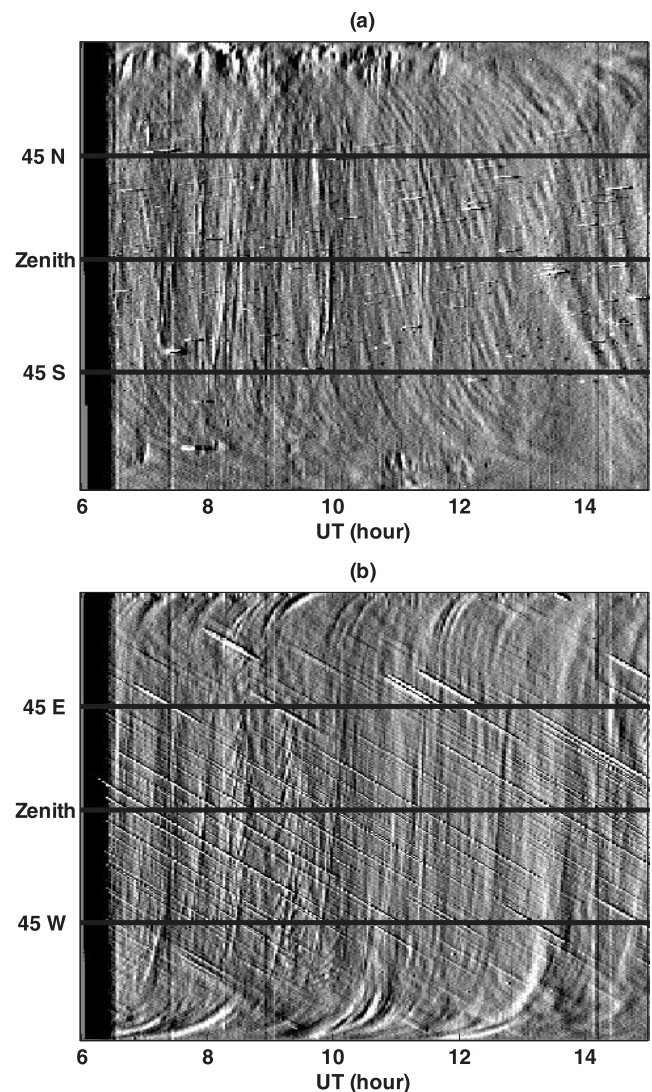

(a)

(b)

Figure 2. (a) North-south and (b) east-west keograms for 28 October 2003, Maui, HI. The N-S (E-W) keogram is generated by taking a vertical (horizontal) column (row) from the center of individual TD images and by placing the columns (rows) side by side sequentially.

and intrinsic frequencies known, the perturbations in original images were readily calculated. Since the time interval for TD image generation was 2 min, the process acts as a high-pass filter in time domain, which favors identification of short period (6 to ∼40 min) waves. These high-frequency waves make the main contribution to the momentum flux budget [*Swenson et al.*, 1999; *Vincent and Reid*, 1983]. Finally, the undisturbed airglow intensity was estimated from the original images with CCD dark current and optical background removed. After the above processes had been accomplished, the gravity wave dispersion relation was used to compute the vertical wavelength for each wave [*Hines*, 1960], and the momentum fluxes were calculated for vertically propagating waves.

3. Experimental Results

[7] In this study, we have processed OH airglow images with meteor radar winds taken simultaneously in January, April, July, and October 2003, from Maui, HI. We first present the results from 28 October 2003, with a detailed analysis of gravity wave features and variations for this single night. Following this one night analysis, the results of the processed months are presented. The statistical and seasonal trend information is then compared with earlier results.

3.1. The 28th of October 2003, Maui, HI

[8] The momentum fluxes of recognizable quasi-mono-chromatic wave components were calculated for every three consecutive images. In the group of three images, the momentum flux estimation is the vector summation of the momentum fluxes of all the vertically propagating wave components if one or more waves are identified. Figure 1 presents the nightly scatterplot with each point representing the vector sum of momentum fluxes of all wave components in a 6-min time interval associated with the three images used in the calculation. This plot shows that most of the waves were propagating to the south, which is also seen from the wave pattern direction in the north-south keogram (Figure 2a; the waves initially appear in the north, pass overhead, and then travel southward). As shown in Figure 1, there are many waves carrying small momentum fluxes and also several waves with momentum fluxes much larger than the mean value (zonal mean = −1.68 m²/s², meridional mean = −4.32 m²/s²). The momentum flux magnitude variation versus time is presented in Figure 3. In this plot, error bars of momentum fluxes for some single wave times (only one wave is recognized at that time) are plotted. The uncertainty for a calculated wave momentum flux is estimated from Monte Carlo simulation with the extracted wave parameters used to generate synthetic wave propagation. Poisson noise is added to the ideal images to simulate the CCD optical system effect. The error given for each momentum flux magnitude is the result of uncertainties in the extraction of horizontal wavelength, phase speed, and wave amplitude. Figure 3 reveals a significant increase in momentum flux after 11 universal time (UT). This trend is well reflected in the keograms (Figure 2), which show stronger wave perturbation patterns after 11 UT than before.

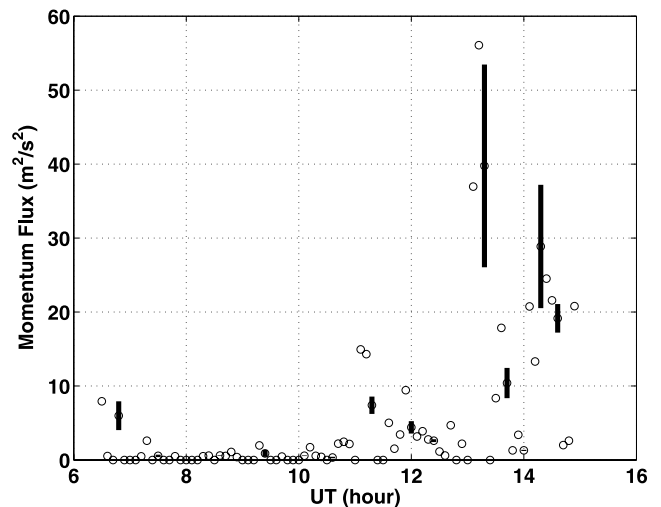[9] To further explore the gravity wave properties, we present the plots in Figure 4 for understanding the con-

Figure 3. Momentum flux magnitude variation over the night of 28 October 2003, Maui, HI. Each point represents the magnitude of the momentum flux carried by all propagating wave components within a 6-min time interval. Error bars are shown for some of the times when only one wave is identified.

nections among the extracted wave parameters and their relation to the wave momentum flux. Figure 4a is a diagram showing the intrinsic phase speed versus horizontal wavelength. We choose 15 km and 60 km as the lower and upper limits of vertical wavelength to select waves for estimating momentum fluxes. The 15 km lower limit is a conservative estimate of the shortest vertical wavelength wave that OH imagers are capable of observing. Ground observations of airglow intensity perturbation caused by waves with short vertical wavelengths are smaller than they really are because of cancellation of opposite wave perturbation within the airglow layer. As such, a large uncertainty arises in the momentum flux estimation for these waves. However, waves with vertical wavelength longer than 60 km are very close to being evanescent. Among 120 waves identified, 76 have vertical wavelength between 15 km and 60 km; 26 have vertical wavelength shorter than 15 km, 12 longer than 60 km, and 6 imaginary (evanescent). In Figure 4b, the extracted wave perturbation in the original images is plotted versus wave period. The line in the plot shows the average wave perturbation amplitude that can be identified for waves with different periods. The values on the line are estimated from 10% of the average TD image energy from the night of 28 October 2003. As stated in the work of *Tang et al.* [2005], a wave component has to cover more than 10% energy in the TD images to be confidently identified in a cross periodogram. Obviously, longer period waves have to be stronger than shorter period waves to be equally identified as a result of the TD process, which acts as a high-pass filter in time domain. For example, the perturbation amplitude of a 40-min wave has to be more than 5 times that of a 6-min wave in order to be recognized. Figure 4c shows that waves with short vertical wavelengths carry a large range of momentum fluxes while the momentum fluxes carried by waves with longer vertical wavelengths are relatively small. The momentum fluxes estimated for the
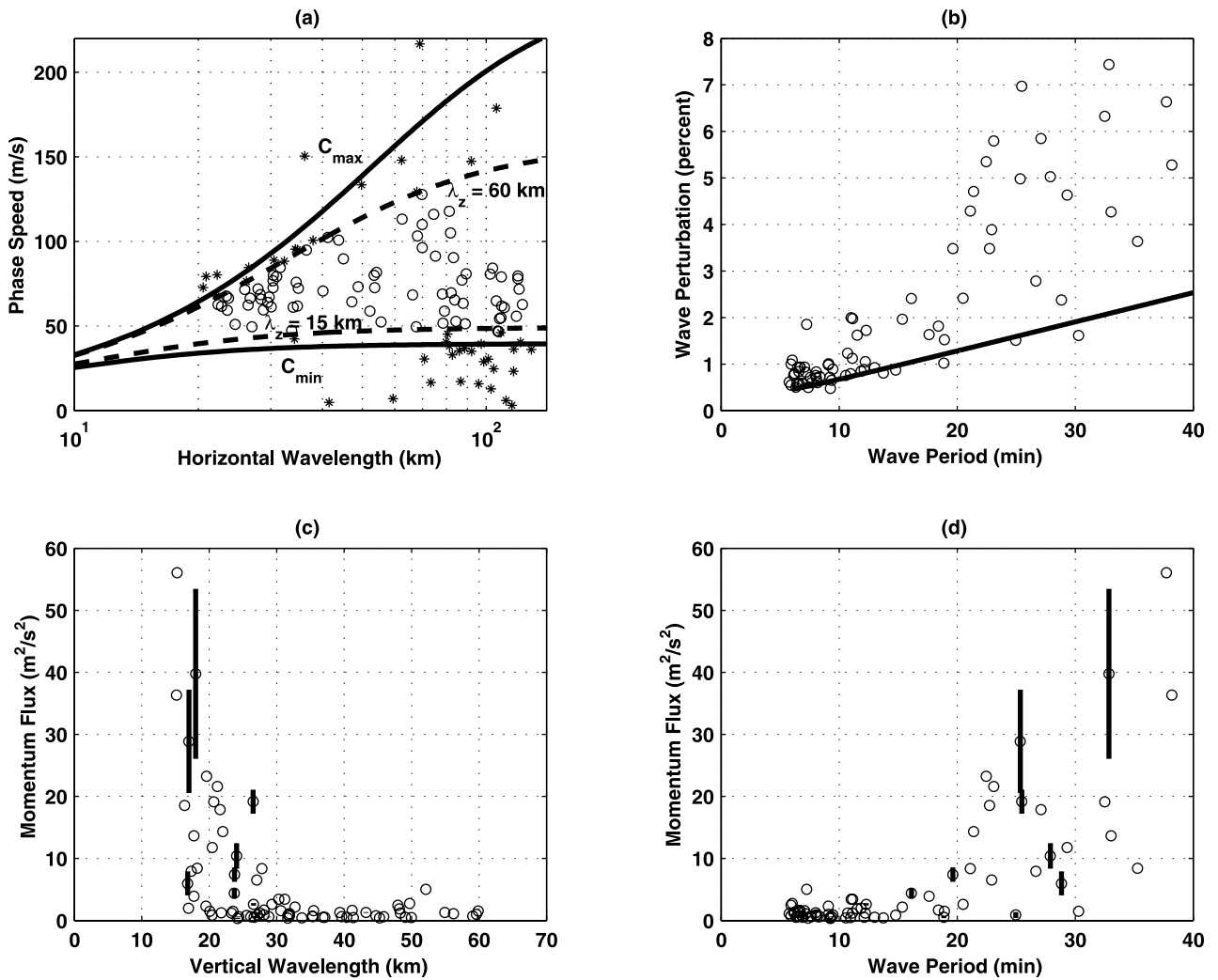
Figure 4. Relations between wave parameters and momentum flux for 28 October 2003, Maui, HI. (a) Plot of wave intrinsic phase speed versus horizontal wavelength. Every circle point represents one wave component with vertical wavelength within 15–60 km range. Each star point represents a wave component out of this range. The solid curves C_{max} and C_{min} are derived from the dispersion relation using $\lambda_z = \infty$ and $\lambda_z = 12$ km as presented in the work of *Swenson et al.* [2000]. The dashed curves are derived using $\lambda_z = 60$ km and $\lambda_z = 15$ km, which are the upper and lower limits of the vertical wavelength of waves for momentum flux calculation, respectively. (b) Plot of airglow perturbation amplitude versus wave period. The line represents the average smallest wave perturbation that can be confidently recognized at the given wave period. (c) Plot of momentum flux magnitude versus vertical wavelength. Error bars of some wave momentum fluxes are shown. (d) Plot of momentum flux magnitude versus wave period. Error bars of some wave momentum fluxes are shown.
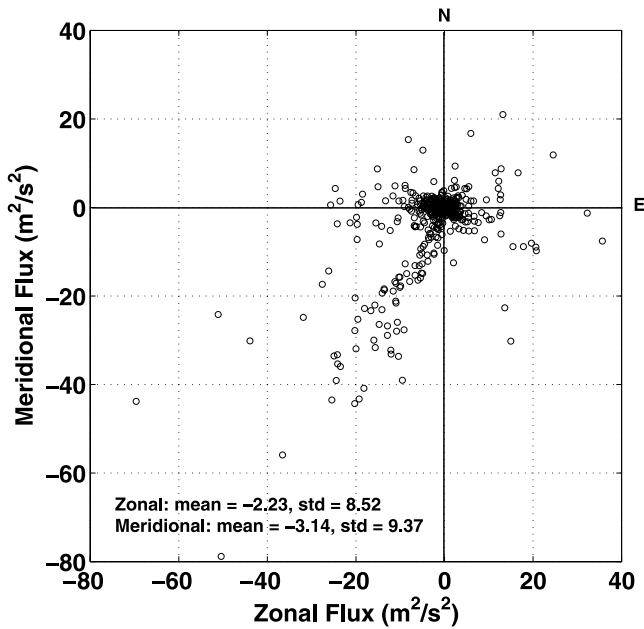
Figure 5. Scatterplot of momentum fluxes for October 2003, Maui, HI. The points have the same meaning as those in Figure 1, except that these are for all observations taken in October 2003, which include 10 nights.
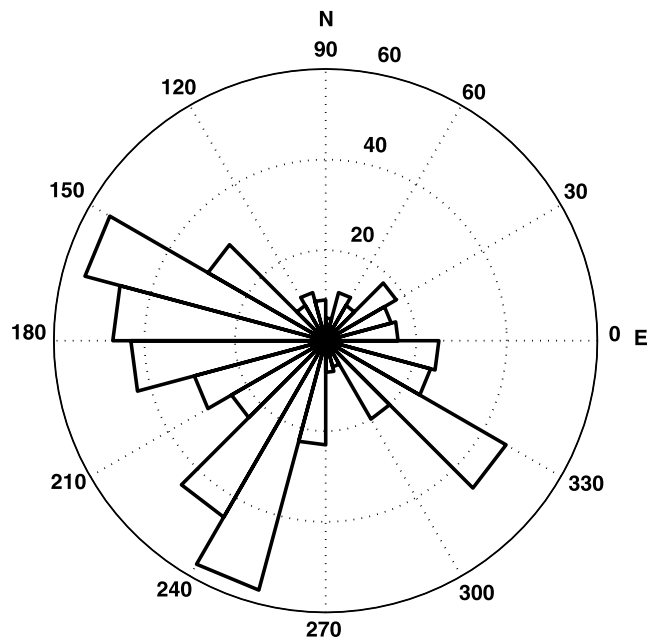

Figure 7. Polar histogram of momentum flux directions for October 2003, Maui, HI. Each petal represents the number of wave components (points in Figure 5) propagating in the direction range.

short vertical wavelength waves (<20 km) generally have larger uncertainties as the cancellation factor (CF) is small, as shown by the error bars of some selected waves with different vertical wavelengths. The CF, which relates the measured airglow intensity to the relative atmospheric density perturbation and consequently to the wave amplitude, is a measure of the cancellation effect. A smaller CF represents stronger cancellation [*Liu and Swenson*, 2003]. Momentum flux magnitude involves the combined effect of the horizontal and vertical wavelengths, the wave perturbation amplitude, and the CF. Figure 4d shows that wave components detected with longer periods generally carry

greater momentum fluxes (and also have larger uncertainties) than those with shorter periods.

3.2. Statistical Results

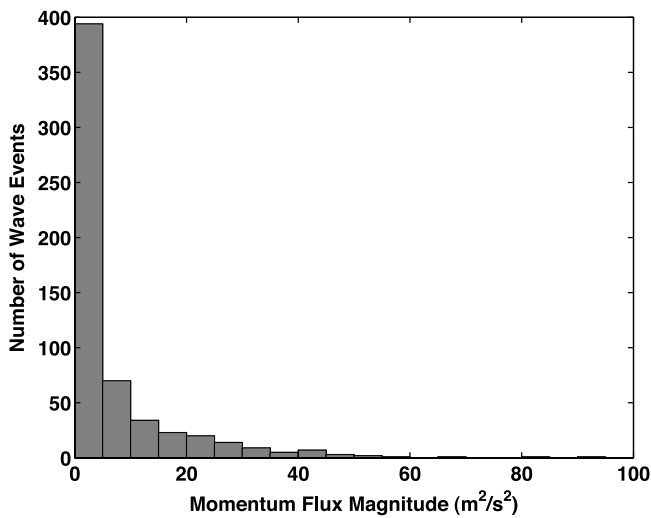[10] As mentioned above, data from clear nights in January, April, July, and October 2003 from Maui, HI, have

Figure 6. Histogram of momentum flux magnitudes for October 2003, Maui, HI. Each column represents the number of wave components.
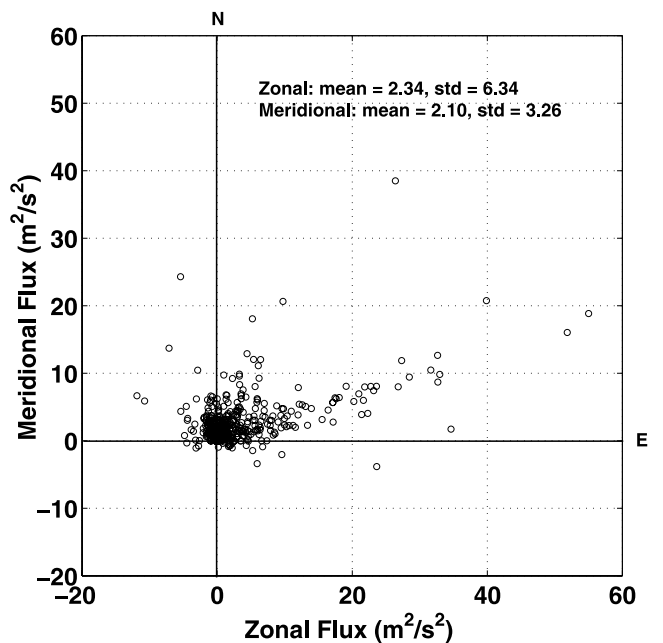

Figure 8. Scatterplot of momentum fluxes for April 2003, Maui, HI. The points have the same meanings as those in Figure 5, except that these are for the observations taken in April 2003, which include 8 nights.
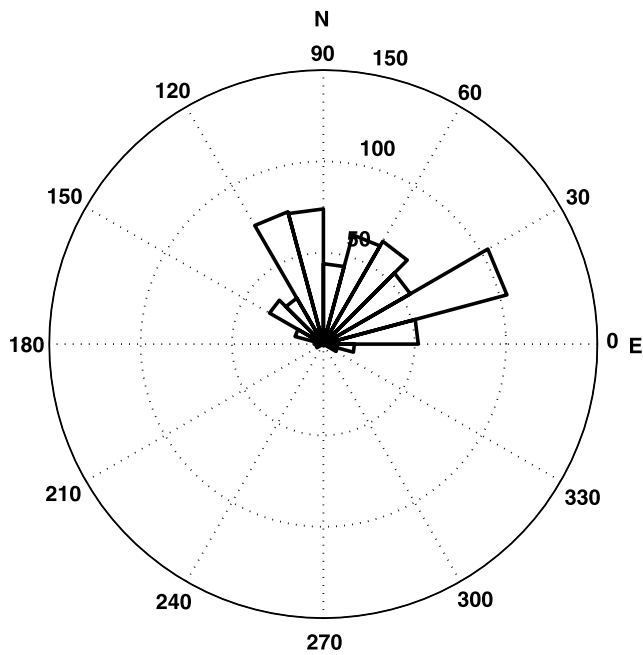
Figure 9. Polar histogram of momentum flux directions for April 2003, Maui, HI. Each petal represents the number of wave components (points in Figure 8) propagating in the direction range.

been processed using the newly developed momentum flux estimation technique. We classify these four months into summertime (21 March to 22 September) and wintertime (23 September to 20 March) measurements [*Tang et al.*, 2002]. According to the classification of the data the wave distribution is different in the different seasons. This effect could be caused by the filtering of the wave spectrum due to
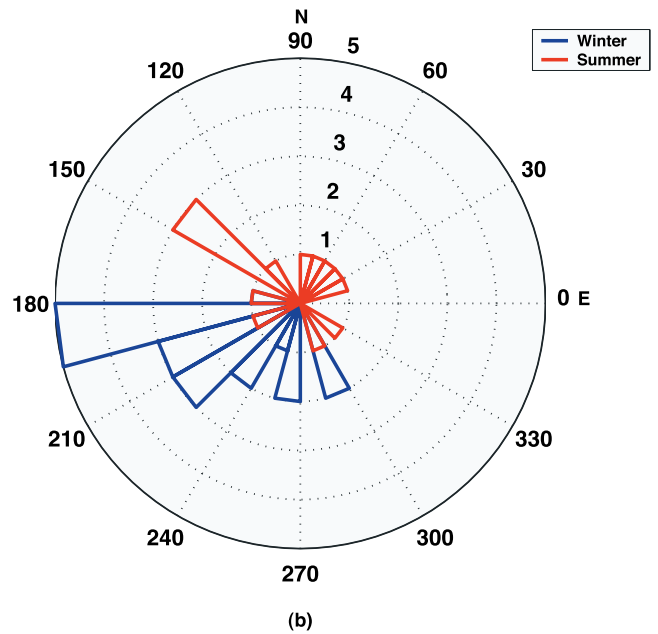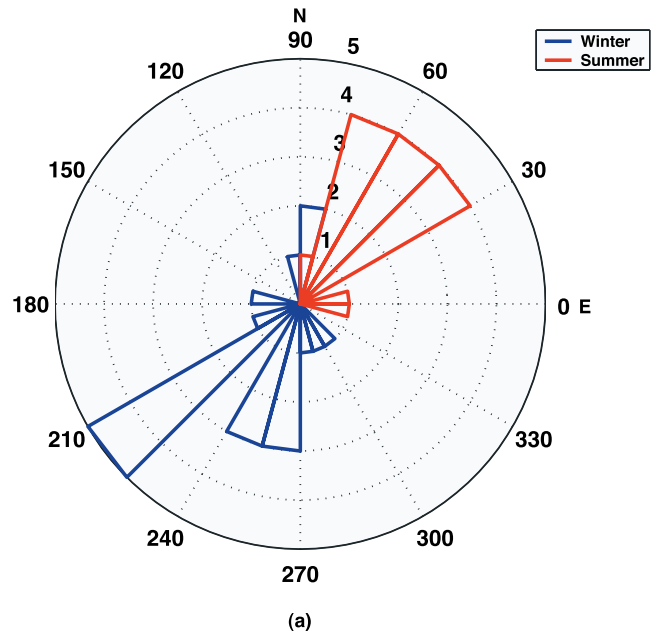

Figure 10. Scatterplot of nightly mean momentum fluxes for January, April, July, and October 2003, Maui, HI. Each diamond point represents the momentum flux of one night. The two square points are the average momentum fluxes of the summer and winter momentum fluxes, respectively. The bars represent the standard deviations of the momentum fluxes in zonal and meridional directions. They are measures of the dispersions of the momentum fluxes.

(a)

(b)

Figure 11. Polar histograms of nightly average wave propagation directions for (a) Maui, HI, 2003 and (b) SOR, NM, 1998–2000. In both locations the momentum flux direction has a southwest preference in winter and a north preference in summer.
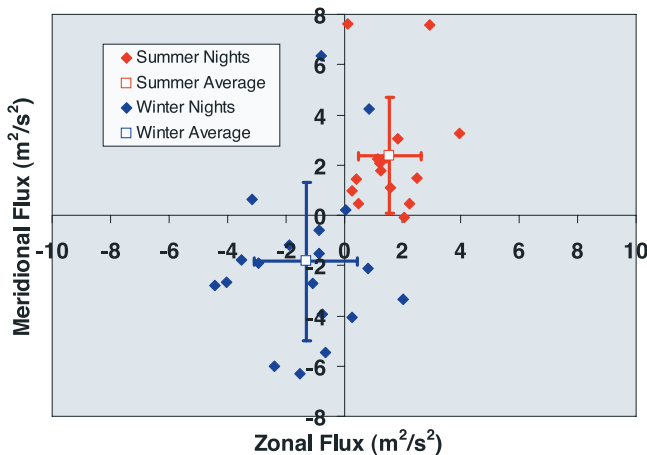
the lower atmospheric wind fields which are different in the different seasons. Scatterplots and histograms of individual wave propagation directions of April and October are presented for comparison of these two months belonging to different seasons.

[11] Figure 5 is the scatterplot for all the processed data of October, with each point representing one wave component. The vector average of the momentum flux in this period has a southwest direction (zonal mean = -2.23 m^2/s^2, meridional mean = -3.14 m^2/s^2). Figure 6 shows a histogram of momentum flux magnitude. Most of

the waves (over 90%) carry small momentum fluxes (less than 10 m^2/s^2) and waves with large momentum fluxes are a small portion of the total. Figure 7 is the polar histogram of wave propagation directions. The reason for presenting the number of waves propagating in each direction is that even in a case with large uncertainty in the momentum flux magnitude, the direction of the wave is well determined. More specifically, the uncertainties in the wave propagation azimuth angles are shown to be less than 1° for all the selected waves in the Monte Carlo simulations mentioned above. In Figure 7, the southwest quadrant has the largest number of waves with northwest, southeast, and northeast quadrants having fewer waves. In contrast to the dominant October wave direction, most of the April waves propagate to the north and the average momentum flux has a northeast direction as presented in Figure 8. Figure 9 shows that more waves propagate in the northeast direction than in the northwest direction and only isolated waves have a southward component.

[12] The nightly means of all the processed nights (from January, April, July, and October 2003) are presented in the scatterplot in Figure 10, separated into summer and winter seasons. Most of the summer nights have an average momentum flux directed toward the northeast and winter nights to the southwest. This directionality is similar to what has been presented by *Tang et al.* [2002] for seasonal variations of gravity waves observed in SOR, NM. The polar histograms of nightly mean wave propagation directions for processed Maui nights and SOR nights are shown in Figure 11. In SOR data, the waves propagate exclusively in the southwest during the winter season and the waves propagate predominately northward in summer. For SOR, the momentum fluxes of 32 nights (from 3 years in SOR) were estimated using the *Gardner et al.* [1999] method, which estimates momentum flux using the RMS values of horizontal and vertical wind perturbations measured by lidar and the correlation coefficients extracted from OH images. The momentum flux calculated covers waves with horizontal wavelengths be-
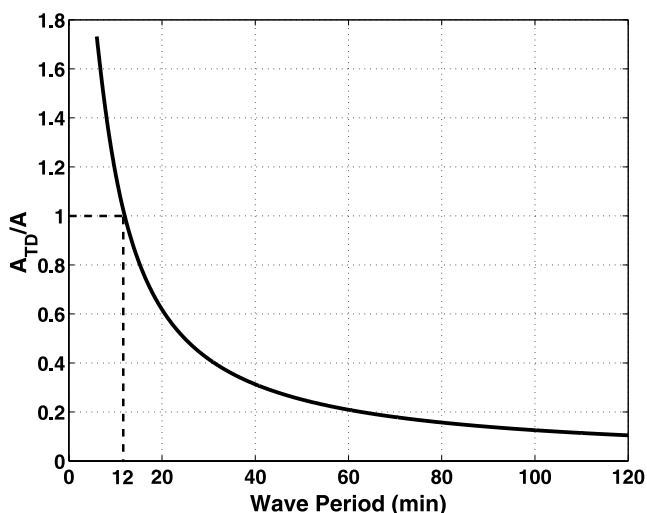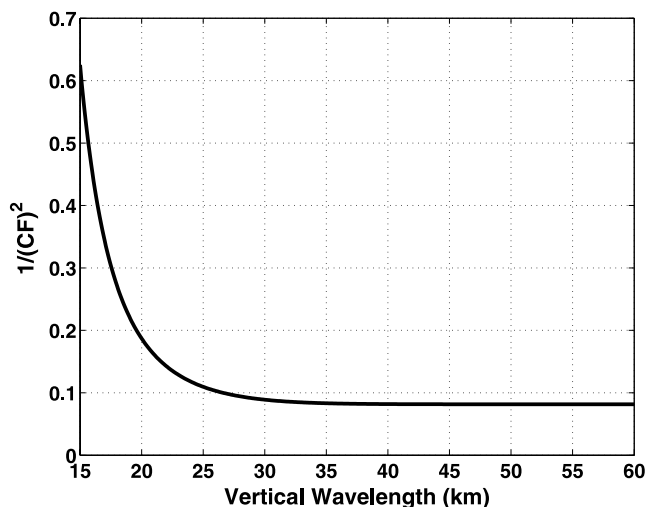

Figure 13. Plot of $1/(CF^2)$ versus vertical wavelength. The curve shows that the cancellation effect on momentum flux varies at a fast rate when the vertical wavelength is shorter than 20 km.

tween 2.4 km and 150 km and observed periods between 4 min and 2 hours [*Gardner et al.*, 1999].

4. Discussion

[13] A new technique has been developed for extracting momentum flux from airglow images [*Tang et al.*, 2005]. The new technique identifies individual wave components and extracts intrinsic wave parameters objectively. As a result, it distinguishes between vertically propagating and evanescent waves prior to calculation of momentum flux. The new method isolates the high-frequency wave events. There is no assumption of spectral shape of the total horizontal wind variance as required by the *Gardner et al.* [1999] method. Aside from providing nightly averages of momentum flux, the method presents the nightly variation of momentum flux magnitude and direction.

[14] We have used the newly developed method to estimate high frequency gravity wave momentum flux with four months of imager data and meteor wind data taken at Maui, HI, 2003. The results of individual nights (e.g., 28 October 2003) have been analyzed in depth. As presented by *Swenson et al.* [2000], dispersion imposes limits on the physical properties of gravity waves. For a vertically propagating wave with certain horizontal wavelength, its intrinsic phase speed has a lower and an upper limit. In a typical night such as 28 October 2003, for those waves we have confidence in identifying (vertical wavelength longer than 15 km), a majority (88 out of 94) of the waves are vertically propagating waves.

[15] We have mentioned earlier that the method favors short period wave identification because the 2-min TD process acts as a high pass filter. Furthermore, the uncertainty of the estimated intensity perturbation varies for different period waves when the waves have the same energy (wave amplitude) in the periodograms of TD images. This is because the ratio of the TD to original wave amplitudes varies. Using Monte Carlo simulation, we have estimated that the standard deviation of an extracted 1%

Figure 12. Ratio of wave amplitude in the TD image (A_{TD}) to that in the original images (A) with 2-min time interval.

perturbation in TD images is 0.04%. The ratio of the TD to original wave amplitudes versus wave period is shown in Figure 12. It shows that the uncertainty for a 12 min wave with 1% perturbation in TD images has the same uncertainty in the original images since it has the same perturbation in the original and the TD images. The perturbation of a 40 min wave with 1% perturbation in TD images is estimated to have a 3.2% perturbation in the original images with the uncertainty being 0.13%. This implies that for those relatively long period waves, the uncertainties for the intensity perturbation estimation is larger than those for the short period waves.

[16] On the 28 October 2003 night, the relation between momentum fluxes and vertical wavelengths indicated that larger momentum fluxes occurred in the short vertical wavelength cases, which was analyzed considering the cancellation effect in the airglow layer. For waves with vertical wavelengths (λ_z) shorter than 20 km, uncertainties in λ_z generate large uncertainty in the CF, which is further magnified in the momentum flux estimation (refer to Figure 4c). As the momentum flux magnitude is proportional to $1/CF^2$ [*Swenson and Liu*, 1998, equation (9)], the $1/CF^2$ versus vertical wavelength plot (Figure 13) is presented showing the large change of cancellation effect in the region of vertical wavelength shorter than ~20 km. (Note that we used the analytical CF formula fit by *Swenson and Liu* [1998] in this momentum flux study. The new CF model presented in the work of *Liu and Swenson* [2003] has been applied to 28 October 2003 data, i.e., results presented in Figures 1, 2 and 4, and the resulted difference between the nightly average momentum fluxes is ~10%. The analytical fit for the new CF model is being implemented.)

5. Summary

[17] To estimate the momentum flux of high-frequency gravity waves from airglow images and background winds, a novel technique for wave identification and wave parameter extraction has been developed. It does not depend on high-resolution lidar measurements as required by the *Gardner et al.* [1999] method. Using this new technique, we have analyzed 34 nights of data taken in four months from 2003 at Maui, HI. The statistical result indicates that the seasonal (two months in summer and two in winter) direction of momentum flux at Maui is predominantly southwestward in winter and northeastward in summer. The zonal preference of wave propagation in this study using data from the low latitude station (20.7°N, 156.3°W) is the same as that reported by *Walterscheid et al.* [1999] (35°S, 138°W) and *Nakamura et al.* [2001] (35°N, 136°E). This suggests that gravity waves extracted by the new technique (20–120 km horizontal wavelength, 6–40 min period) are generated in the lower troposphere and propagate into the MALT region, filtered by the middle atmosphere zonal wind, which is strong in the eastward (westward) direction in winter (summer). In the meridional direction, the wave propagation preference is toward the summer pole, which is the same as what has been reported for other locations [*Walterscheid et al.*, 1999; *Nakamura et al.*, 2001; *Tang et al.*, 2002]. This directional trend of the meridional waves found in these studies is very intriguing. It is likely that this meridional wave flux applied a stress on the mean meridional wind, similar to the zonal wave stress on the zonal wind.

References

Franke, S. J., X. Chu, A. Z. Liu, and W. K. Hocking (2005), Comparison of meteor radar and Na Doppler lidar measurements of winds in the mesopause region above Maui, Hawaii, *J. Geophys. Res.*, 110, D09S02, doi:10.1029/2003JD004486.

Gardner, C. S., K. Gulati, Y. Zhao, and G. R. Swenson (1999), Measuring gravity wave momentum fluxes with airglow images, *J. Geophys. Res.*, 104, 11,903–11,915.

Hines, C. O. (1960), Internal atmospheric gravity waves at ionospheric heights, *Can. J. Phys.*, 38, 1441–1481.

Liu, A. Z., and G. R. Swenson (2003), A modeling study of O_2 and OH airglow perturbations induced by atmospheric gravity waves, *J. Geophys. Res.*, 108(D4), 4151, doi:10.1029/2002JD002474.

Nakamura, T., T. Tsuda, R. Maekawa, M. Tsutsumi, K. Shiokawa, and T. Ogawa (2001), Seasonal variation of gravity waves with various temporal and horizontal scales in the MLT region observed with radar and airglow imaging, *Adv. Space Res.*, 27, 1737–1742.

Schubert, G., and R. L. Waterscheid (1988), Wave-driven fluctuations in OH nightglow from an extended source region, *J. Geophys. Res.*, 93, 9903–9915.

Swenson, G. R., and C. S. Gardner (1998), Analytical models for the responses of the mesospheric OH* and Na layers to atmospheric gravity waves, *J. Geophys. Res.*, 103, 6271–6294.

Swenson, G. R., and A. Z. Liu (1998), A model for calculating acoustic gravity wave energy and momentum flux in the mesosphere from OH airglow, *Geophys. Res. Lett.*, 25, 477–480.

Swenson, G. R., R. Haque, W. Yang, and C. S. Gardner (1999), Momentum and energy fluxes of monochromatic gravity waves observed by an OH imager at Starfire Optical Range, New Mexico, *J. Geophys. Res.*, 104, 6067–6080.

Swenson, G. R., M. J. Alexander, and R. Haque (2000), Dispersion imposed limits on atmospheric gravity waves in the mesosphere: Observations from OH airglow, *Geophys. Res. Lett.*, 27, 875–878.

Tang, J., A. Z. Liu, and G. R. Swenson (2002), High-frequency gravity waves observed in OH airglow at Starfire Optical Range, NM: Seasonal variations in momentum flux, *Geophys. Res. Lett.*, 29(20), 1966, doi:10.1029/2002GL015794.

Tang, J., F. Kamalabadi, S. J. Franke, A. Z. Liu, and G. R. Swenson (2005), Estimation of gravity wave momentum flux with spectroscopic imaging, *IEEE Trans. Geosci. Remote Sens.*, 43(1), 103–109.

Tarasick, D. W., and C. O. Hines (1990), The observable effects of gravity waves on airglow emissions, *Planet. Space Sci.*, 38, 1105–1119.

Vincent, R. A., and I. M. Reid (1983), HF Doppler measurements of mesospheric gravity wave momentum fluxes, *J. Atmos. Sci.*, 40, 1321–1333.

Walterscheid, R. L., J. H. Hecht, R. A. Vincent, I. M. Reid, J. Woithe, and M. P. Hickey (1999), Analysis and interpretation of airglow and radar observations of quasi-monochromatic gravity waves in Adelaide, Australia (35°S, 138°E), *J. Atmos. Terr. Phys.*, 61, 461–478.

————————————

F. Kamalabadi, A. Z. Liu, G. R. Swenson, and J. Tang, Department of Electrical and Computer Engineering, University of Illinois at Urbana-Champaign, 1308 W. Main St., Urbana, IL 61801, USA. (farzadk@uiuc.edu; liuzr@uiuc.edu; swenson1@uiuc.edu; jingtang@uiuc.edu)